

Tunable plasmon-enhanced second-order optical nonlinearity in transition-metal-dichalcogenide nanotriangles

F. Karimi,* S. Soleimanikahnoj,† and I. Knezevic‡

Department of Electrical and Computer Engineering,
University of Wisconsin-Madison, Madison, Wisconsin 53706, USA

The development of nanomaterials with a large nonlinear susceptibility is essential for nonlinear nanophotonics. We show that transition-metal-dichalcogenide (TMD) nanotriangles have a large effective second-order susceptibility $[\chi^{(2)}]$ at mid-infrared to near-infrared frequencies owing to their broken centrosymmetry. $\chi^{(2)}$ is calculated within the density-matrix formalism that accounts for dissipation and screening. $\chi^{(2)}$ peaks in the vicinity of both two-photon resonances (specified by the geometry) and plasmon resonances (tunable via the carrier density). Aligning the resonances yields the values of $\chi^{(2)}$ as high as 10^{-6} m/V. These findings underscore the potential of TMD nanotriangles for nonlinear nanophotonics, particularly second-harmonic generation.

Nonlinear frequency conversion processes, such as second-harmonic generation (SHG) and third-harmonic generation, have many applications in nanophotonics [1–6]. These phenomena rely on intrinsically weak matter-mediated photon–photon interactions [7–9], which can be enhanced through a number of techniques, such as dielectric confinement through Mie resonances [10, 11], quantum confinement [12–17], and surface-plasmonic field enhancement [9, 18–24].

The nonlinear and plasmonic response of two-dimensional materials, such as graphene [25–40] and transition-metal dichalcogenides (TMDs) [41–46], has been attracting interest for nonlinear optical applications [47, 48]. In TMDs with an odd number of layers, there is weak SHG owing to the material’s broken centrosymmetry [44, 46]. In recent years, excitonic effects in TMDs [49] have been shown to greatly amplify SHG [50–52].

It is challenging to achieve plasmonic-field enhancement in two-dimensional materials because the plasmon wave vector far exceeds that of light at the same frequency. One solution is to lower the system dimensionality, from two to zero. Indeed, quasi-zero-dimensional structures support standing plasmonic resonances that can be easily excited and have been shown to yield an enhanced nonlinear response of graphene nanoislands and nanotriangles [9, 18–20]. It is important to note that noncentrosymmetric shapes, such as triangles, aid SHG [16, 17].

In this Letter, we show that equilateral nanotriangles made of single-layer TMDs such as MoS₂, WS₂, and WSe₂, whose growth has already been demonstrated [53–57], have a strong and electrically tunable second-order nonlinear optical response at midinfrared (mid-IR) to near-infrared (near-IR) frequencies. We calculate the second-order nonlinear optical response of these systems within the density-matrix framework that accounts for

screening and dissipation [1] (excitonic effects are not considered). We show that the second-order susceptibility peaks in the vicinity of both two-photon intersubband resonances (whose positions are fixed by the nanotriangle geometry) and plasmon resonances (dynamically tunable by the carrier density). By tuning the carrier density to bring the plasmon and two-photon resonances into alignment, second-order susceptibility $\chi^{(2)}$ can become as high as 10^{-6} m/V, orders of magnitude higher than the intrinsic SHG of single-layer TMDs ($\sim 10^{-9}$ m/V) or the second-order susceptibility of bulk LiNbO₃ ($\sim 10^{-11}$ m/V) at near-IR frequencies [48, 58]. The second-order optical response increases as the triangle size decreases. These findings underscore the suitability of single-layer TMD nanotriangles as elements for nonlinear nanophotonics.

Density-Matrix Calculation. TMDs have the general formula of MX_2 , with M and X representing a transition metal and a chalcogen, respectively. Single-layer MX_2 (M =Mo, W; X =S, Se) are direct-bandgap semiconductors [59]. Since these TMDs have very similar electron effective masses (between 0.46 and 0.55 m_e), same-size nanotriangles of them are expected to have similar optical responses. Therefore, in this paper, we only study the second-order nonlinear response of MoS₂ nanotriangles (effective mass 0.55 m_e [59]).

Using the density-matrix method [1], we calculate the loss function and second-order susceptibility for an MoS₂ equilateral nanotriangle with the side length L , area A , thickness d , and sheet carrier density n_s . The nanotriangle lies on the $z = 0$ plane upon a substrate that fills the $z < 0$ half-space and has an absolute dielectric permittivity $\varepsilon_b = \varepsilon_0 \kappa_b$. We assume the nanotriangle is illuminated with TM-polarized light with the electric field along the y -direction [Fig. 1(a)]. A similar theoretical approach was successfully employed for graphene nanoflakes [9, 18].

The Hamiltonian describing electrons in a TMD nanotriangle is $\mathbb{H} = \mathbb{P}^2/2m_e + \mathbb{U}_L + \mathbb{U}_W$. \mathbb{U}_L is the lattice potential and \mathbb{U}_W denotes a mesoscopic-scale potential defining the triangle (zero within and infinite elsewhere). The details of the tight-binding representation of the lattice potential \mathbb{U}_L can be found in Refs. [60–62], while the

* farhadk@gmail.com

† si.soleimani@gmail.com

‡ iknezevic@wisc.edu

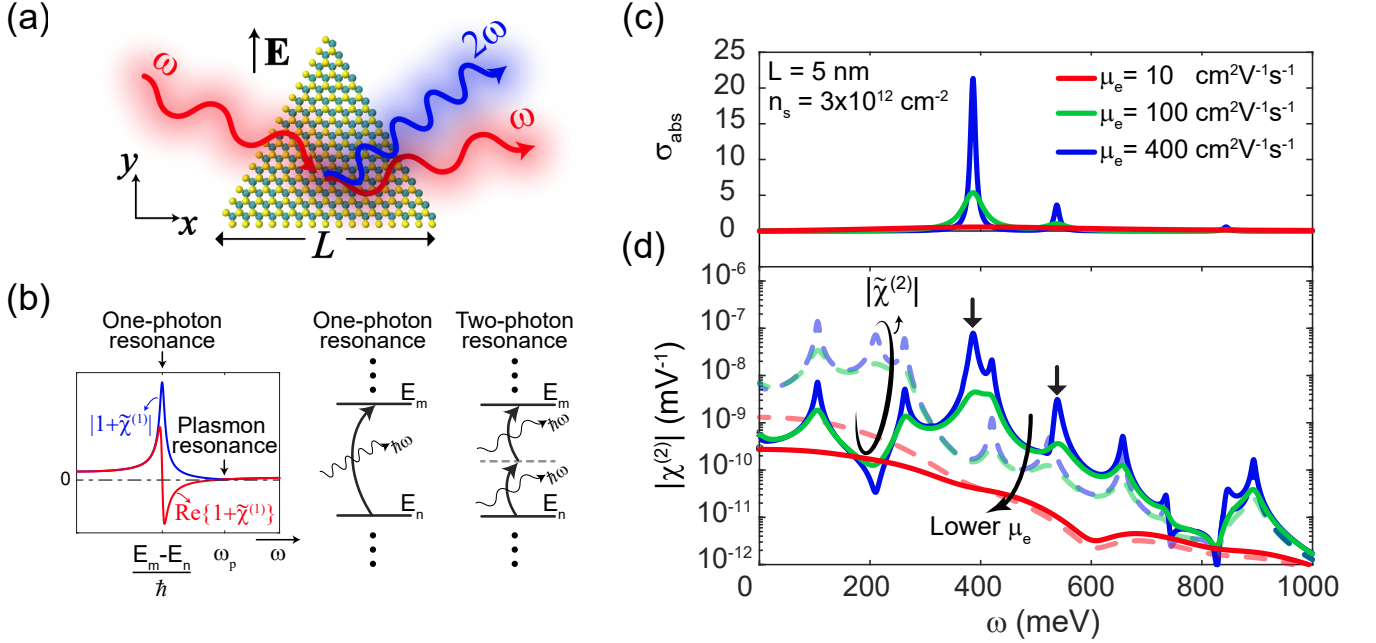


FIG. 1. (a) Schematic of an equilateral TMD nanotriangle with the side length L . TM-polarized incident light causes linear as well as second-order nonlinear optical response. (b) One-photon, two-photon, and plasmon resonances. One- and two-photon resonances are due to intersubband optical transitions, whereas plasmon resonances are due to collective oscillations of electrons. (c) The loss function and (d) second-order susceptibility in response to external field (solid) and total field (dashed) of a 5-nm TMD nanotriangle with the sheet density $n_s = 3 \times 10^{12} \text{ cm}^{-2}$ for different values of the electron mobility. The peaks marked by arrows correspond to two different plasmon resonances.

database presented in Ref. [59] provides details on the TMD electronic structure, including effective masses. In this paper, we use the envelope-function approximation (EFA), which, given the size of the nanotriangles of interest, is an accurate approximation. Using the EFA, the energies and eigenstates of the Hamiltonian are, respectively, $\epsilon_{nm,\nu} = \epsilon_\nu + 8\pi^2\hbar^2/(9m_\nu^*L^2)(n^2 + m^2 + nm)$ and $\langle \mathbf{r} | nm, \nu \rangle = f_{nm}(\mathbf{r})u_\nu(\mathbf{r})$. m_ν^* is the electron effective mass near the extremum of the bulk single-layer TMD's ν^{th} band, with the extremum energy ϵ_ν and the periodic part of the Bloch wave function $u_\nu(\mathbf{r})$. $f_{nm}(\mathbf{r})$ is a solution to the Schrödinger equation for a particle in an equilateral triangle, which can be obtained analytically, as detailed in Refs. [63, 64]. The $f_{nm}(\mathbf{r})$ eigenfunctions fall into two classes:

$$f_{nm}^{(1)}(x, y) = N_1 \left\{ \sin[\beta(n+2m)\tilde{x}] \sin[\sqrt{3}\beta n\tilde{y}] + \sin[\beta(m-n)\tilde{x}] \sin[\sqrt{3}\beta(n+m)\tilde{y}] - \sin[\beta(2n+m)\tilde{x}] \sin[\sqrt{3}\beta m\tilde{y}] \right\}, \quad (1a)$$

$$f_{nm}^{(2)}(x, y) = N_2 \left\{ -\cos[\beta(n+2m)\tilde{x}] \sin[\sqrt{3}\beta n\tilde{y}] + \cos[\beta(m-n)\tilde{x}] \sin[\sqrt{3}\beta(n+m)\tilde{y}] - \cos[\beta(2n+m)\tilde{x}] \sin[\sqrt{3}\beta m\tilde{y}] \right\}, \quad (1b)$$

where $\beta = 2\pi/3L$, $\tilde{x} = x + L/2$, $\tilde{y} = y + \sqrt{3}L/2$, and the origin of the Cartesian coordinate system is at the triangle's center. For the eigenfunctions of the first class, $m \geq n > 0$. $N_1 = 2(16/27)^{1/4}/L$ and $N_1 = 2(4/27)^{1/4}/L$ for $m \neq n$ and $m = n$, respectively. For the eigenfunctions of the second class, $m > n > 0$ and $N_2 = 2(16/27)^{1/4}/L$. It should be noted that the EFA is a valid approximation as long as the number of local maxima of a relevant wave function is much smaller than the number of unit cells in the nanotriangle.

Now, once we know the electronic energies and eigenstates in the TMD nanotriangle, we use the density-matrix method to calculate the linear and second-order nonlinear optical susceptibility [1, 9, 18]. The linear optical susceptibility can be obtained from

$$\tilde{\chi}_{ij}^{(1)}(\omega) = \frac{n_s}{\epsilon_0 d} \sum_{\mathbf{s}\mathbf{s}'} (\rho_{\mathbf{s}'\mathbf{s}'}^{(0)} - \rho_{\mathbf{s}\mathbf{s}}^{(0)}) \frac{\mu_{\mathbf{s}\mathbf{s}'}^j \mu_{\mathbf{s}'\mathbf{s}}^i}{\epsilon_s - \epsilon_{s'} - \hbar\omega - i\hbar\gamma}, \quad (2)$$

where \mathbf{s} denotes a set of quantum numbers $\{n, m, \nu\}$, ijk refer to the Cartesian coordinates, and γ represents the relaxation rate of electrons. $\mu_{\mathbf{s}\mathbf{s}'}$ is the electric dipole transition moment and equals to $\langle \mathbf{s} | (-e)\mathbf{r} | \mathbf{s}' \rangle$. Since $f(\mathbf{r})$ varies much slower than $u(\mathbf{r})$, the expression of μ can be simplified. For interband transitions ($\nu \neq \nu'$), $\langle \mathbf{s} | (-e)\mathbf{r} | \mathbf{s}' \rangle \approx \langle \nu | (-e)\mathbf{r} | \nu' \rangle$; for intraband transitions, ($\nu = \nu'$), $\langle \mathbf{s} | (-e)\mathbf{r} | \mathbf{s}' \rangle \approx \langle nm | (-e)\mathbf{r} | n'm' \rangle$. In Eq. (2), $\rho_{\mathbf{s}\mathbf{s}'}^{(0)} = \delta_{\mathbf{s},\mathbf{s}'} F(\epsilon_s)$ denotes the elements of the unper-

turbed density matrix. F is the Fermi-Dirac distribution function and satisfies $\sum_{\mathbf{s}} F(\epsilon_{\mathbf{s}}) = An_{\mathbf{s}}$.

The second-order (nonlinear optical) susceptibility is given by

$$\begin{aligned} \tilde{\chi}_{ijk}^{(2)}(2\omega) = & \frac{n_{\mathbf{s}}}{2\epsilon_0 d} \sum_{\mathbf{s}'\mathbf{s}\mathbf{s}''} (\rho_{\mathbf{s}''\mathbf{s}'}^{(0)} - \rho_{\mathbf{s}\mathbf{s}''}^{(0)}) \times \\ & \left[\frac{\mu_{\mathbf{s}''\mathbf{s}'}^i \mu_{\mathbf{s}'\mathbf{s}}^j \mu_{\mathbf{s}\mathbf{s}''}^k}{(\epsilon_{\mathbf{s}'} - \epsilon_{\mathbf{s}''} - 2\hbar\omega - i\hbar\gamma)(\epsilon_{\mathbf{s}} - \epsilon_{\mathbf{s}''} - \hbar\omega - i\hbar\gamma)} \right. \\ & + \frac{\mu_{\mathbf{s}''\mathbf{s}'}^i \mu_{\mathbf{s}'\mathbf{s}}^k \mu_{\mathbf{s}\mathbf{s}''}^j}{(\epsilon_{\mathbf{s}'} - \epsilon_{\mathbf{s}''} - 2\hbar\omega - i\hbar\gamma)(\epsilon_{\mathbf{s}} - \epsilon_{\mathbf{s}''} - \hbar\omega - i\hbar\gamma)} \\ & + \frac{\mu_{\mathbf{s}''\mathbf{s}'}^j \mu_{\mathbf{s}'\mathbf{s}}^i \mu_{\mathbf{s}\mathbf{s}''}^k}{(\epsilon_{\mathbf{s}'} - \epsilon_{\mathbf{s}} + 2\hbar\omega + i\hbar\gamma)(\epsilon_{\mathbf{s}} - \epsilon_{\mathbf{s}''} - \hbar\omega - i\hbar\gamma)} \\ & \left. + \frac{\mu_{\mathbf{s}''\mathbf{s}'}^k \mu_{\mathbf{s}'\mathbf{s}}^i \mu_{\mathbf{s}\mathbf{s}''}^j}{(\epsilon_{\mathbf{s}'} - \epsilon_{\mathbf{s}} + 2\hbar\omega + i\hbar\gamma)(\epsilon_{\mathbf{s}} - \epsilon_{\mathbf{s}''} - \hbar\omega - i\hbar\gamma)} \right]. \end{aligned} \quad (3)$$

Because of the particle-hole symmetry in single-layer TMDs, the contributions from interband transitions in Eq. (3) add up to zero. In contrast, intraband optical transitions result in a nonzero $\tilde{\chi}^{(2)}$. Therefore, we pick all eigenstates ν in the first conduction band of the single-layer TMD, within which the Fermi level lies.

Moreover, owing to the D_3 symmetry of equilateral triangles, $\tilde{\chi}_{ij}^{(1)}$ and $\tilde{\chi}_{ijk}^{(2)}$ tensors of the TMD nanotriangles can be simplified [1]. The only nonzero elements of $\tilde{\chi}^{(1)}$ are $\tilde{\chi}_{xx}^{(1)} = \tilde{\chi}_{yy}^{(1)}$ and the only nonzero elements of $\tilde{\chi}^{(2)}$ are $\tilde{\chi}_{yyy}^{(1)} = -\tilde{\chi}_{yxx}^{(1)} = -\tilde{\chi}_{xxy}^{(1)} = -\tilde{\chi}_{xyx}^{(1)}$. In this paper, we only calculate $\tilde{\chi}_{yy}^{(1)}$ and $\tilde{\chi}_{yyy}^{(2)}$ and, to simplify the notation, we drop the y indices henceforth.

There are two types of intersubband optical transitions contributing to the second-order optical response: one-photon transitions corresponding to the terms with $\hbar\omega$ in Eq. (3) and two-photon transitions corresponding to the terms with $2\hbar\omega$ in Eq. (3) [Fig. 1(b)]. The second-order susceptibility peaks when either one-photon or two-photon transitions are nearly resonant. The second-order susceptibility also peaks at the vicinity of the plasmon resonances. Unlike the one- and two-photon resonances, which stem from intersubband optical transitions, plasmon resonances are due to collective electron oscillations. In a confined quantum system with considerable energy-level spacing, like TMD nanotriangles, each one-photon resonance is succeeded by a plasmon resonances, as illustrated in Fig. 1(b). Plasmon resonances are weaker at higher subbands owing to the lower subband carrier densities. Unfortunately, $\tilde{\chi}^{(2)}$ does not capture plasmon resonances, because it is calculated in response to the total field acting on electrons, which consists of the external field and the induced field. In order to capture the plasmonic effect and understand the optical response to the external field rather than the total field, we introduce two

quantities that are relevant in experiment [18, 22, 35]:

$$\begin{aligned} \chi^{(2)} &= \tilde{\chi}^{(2)}/(1 + \tilde{\chi}^{(1)})^2, \\ \sigma_{\text{abs}} &= -\text{Im}\{(1 + \tilde{\chi}^{(1)})^{-1}\}, \end{aligned} \quad (4)$$

σ_{abs} denotes the loss function, which peaks near the plasmon resonances. $\chi^{(2)}$ is also referred to as the second-order susceptibility with respect to the external field. (Note that we have used \sim to denote the susceptibility with respect to the total field.) Unlike $\tilde{\chi}^{(2)}$, $\chi^{(2)}$ does not peak near one-photon resonances and only peaks in the vicinity of plasmon and two-photon resonances. The strength of these resonances are critically dependent on the electron relaxation rate. For small γ , the resonances are sharp. For large γ , scattering-induced broadening practically quenches the resonance. In this paper, we use the electron mobility [$\mu_e = e/(m^*\gamma)$] as a proxy for the characteristic relaxation rate γ due to phonons and impurities within the density-matrix formalism [1, 9, 18].

Results and discussion. Figures 1(c) and 1(d) show the loss function (σ_{abs}) and the second-order susceptibility in response to the external field ($\chi^{(2)}$) as well as to the total field ($\tilde{\chi}^{(2)}$). For a fixed side length L , the optical response of a nanotriangle is dependent on the electron mobility, or, equivalently, the electron relaxation rate. The measured room-temperature electron mobility of bulk single-layer MoS₂ is in the range of 0.5–200 cm²/Vs [65–67]. The lower density of electron states in the nanotriangle with respect to bulk leads to reduced scattering rates; this is a well-known feature of low-dimensional systems [68]. To capture this reduction in the scattering rates, we choose an enhanced value of the maximal effective mobility to be 400 cm²/Vs (twice the highest value measured in bulk) as a representative of the high-carrier-mobility range. By increasing the electron mobility, the effect of optical resonances on the second-order optical response becomes more pronounced. (At low electron mobilities [Figs. 1(c) and 1(d)], spectral broadening weakens the optical resonances and $\chi^{(2)}$ varies smoothly as a function of frequency, *i.e.*, is devoid of resonances.) Henceforth, we focus only on the 400 cm²/Vs mobility results, where the interesting features are most prominent.

As discussed above, $\tilde{\chi}^{(2)}$ (the second-order susceptibility with respect to the total field) peaks in the vicinity of one- and two-photon resonances while $\chi^{(2)}$ (the second-order susceptibility with respect to external field) peaks in the vicinity of two-photon and plasmon resonances. The arrow-marked peaks in Fig. 1(c) correspond to the plasmon resonances. The positions of two-photon resonances are dependent on the single-particle energies in the nanotriangle and are fixed for a given nanotriangle size [Fig. 1(c)]. On the other hand, the positions of plasmon resonances depend on electron energies, but also on the carrier density in the nanotriangle. Therefore, we could dynamically tune the plasmon resonances by changing the carrier density (for example, by using back gating), which suggests that, by aligning the plas-

mon and two-photon resonances, we could amplify the second-order optical susceptibility.

Figures 2(a)–(b) show the loss function σ_{abs} and the second-order susceptibility $\chi^{(2)}$ for different carrier densities. The carrier density at which a plasmon resonance and a two-photon resonance are aligned with each other, $\chi^{(2)}$ increases to as large as 10^{-6} m/V. TMD nanotriangles can therefore have almost five orders of magnitude stronger second-order nonlinearity than bulk LiNbO₃ at near-IR frequencies ($\sim 10^{-11}$ m/V) or the intrinsic second-order response of single-layer SHG ($\sim 10^{-9}$ m/V) [48, 58]. The gray shaded areas in Figs. 2(a) and 2(b) show σ_{abs} and $\chi^{(2)}$ calculated for the carrier densities in the range of 10^{11} – 3×10^{13} cm⁻². Plasmon and one-photon resonances never happen at the same frequency, so there are no-plasmon regions at the vicinity of one-photon resonances [Fig. 1(b)], and, consequently, second-order optical susceptibility $\chi^{(2)}$ decreases in the vicinity of one-photon resonances.

To understand the interplay between these resonances, we define ω_{max} as the frequency at which the maximum second-order susceptibility [$|\chi^{(2)}|_{\text{max}}$] happens in a nanotriangle with a given side length, carrier mobility, and carrier density. It can be seen that ω_{max} [black squares in Figs. 2(c)–(d)] are in close proximity of a plasmon resonance. In Fig. 2(c), filled circles denote the plasmon resonances and the color bar represents their corresponding loss function. By lowering the carrier density, ω_{max} asymptotically decreases to the first one-photon resonance of the nanotriangle. By decreasing the carrier density, the plasmon resonances also weaken and $|\chi^{(2)}|_{\text{max}}$ decreases. Correspondingly, the critical electric field, which is defined as $E_c \equiv |\chi^{(1)}|_{\text{max}}/|\chi^{(2)}|_{\text{max}}$ [red triangles in Fig. 2(d)], decreases with increasing carrier density. The lower the critical electric field, the stronger the second-order nonlinear optical response. At high carrier densities, E_c can be as low as ~ 0.1 kVcm⁻¹, which corresponds to an optical field intensity as low as 0.1 kW/cm².

Finally, we study the effect of the TMD nanotriangle's size on its second-order optical nonlinear response. Figure 3 shows $|\chi^{(2)}(\omega)|$ as a function of frequency and carrier density for nanotriangles with different sizes. By increasing the side length L , the maximum value of $\chi^{(2)}$

decreases. Increasing L has a twofold effect. On one hand, the magnitude of the dipole moments grows with increasing L . On the other hand, the spacing between a nanotriangle's energies drops with increasing L and results in more one- and two-photon processes contributing to the second-order nonlinear response. Since these one- and two-photon processes have different phases, the net effect of these competing phenomena results in the lower $|\chi^{(2)}(\omega)|$ for larger L . Also, owing to the smaller energy spacing, the first horizontal asymptote of ω_{max} occurs at a lower frequency in large nanotriangles.

Conclusion. We showed that, in the mid-IR to near-IR frequency range, TMD nanotriangles have a large and tunable second-order susceptibility, which makes them promising materials for integrated nonlinear-nanophotonics applications. Using the density-matrix method with an account of screening and dissipation, we calculated the linear and second-order optical response of TMD nanotriangles. We showed that second-order susceptibility peaks at the vicinity of plasmon and two-photon resonances. For a given material, the two-photon resonances are fixed by the nanotriangle's size while the plasmon resonances can be tuned via the carrier density. By aligning the plasmon and two-photon resonances, second-order susceptibility can become as high as 10^{-6} m/V, with higher magnitudes found in smaller triangles.

If a triangle deviates from perfect D_3 symmetry, which is relevant in experiment, the second-order nonlinear susceptibility tensor will have more than four nonzero elements. There will be many more nonzero dipole transition moments, meaning more one- and two-photon processes with different phases, which might reduce the second-order nonlinear susceptibility.

Acknowledgment. The authors gratefully acknowledge support by the U.S. Department of Energy, Office of Basic Energy Sciences, Division of Materials Sciences and Engineering, Physical Behavior of Materials Program, under Award DE-SC0008712. Preliminary work was partially supported by the Splinter Professorship. This work was performed using the compute resources and assistance of the UW-Madison Center for High Throughput Computing (CHTC) in the Department of Computer Sciences.

-
- [1] R. W. Boyd, *Nonlinear Optics, Third Edition*, 3rd ed. (Academic Press, 2008).
 - [2] Z. Sun, A. Martinez, and F. Wang, Optical modulators with 2d layered materials, *Nat. Photonics* **10**, 227 (2016).
 - [3] Z. Sun, Electrically tuned nonlinearity, *Nat. Photonics* **12**, 383 (2018).
 - [4] C. Wang, M. Zhang, B. Stern, M. Lipson, and M. Lončar, Nanophotonic lithium niobate electro-optic modulators, *Opt. Express* **26**, 1547 (2018).
 - [5] A. Krasnok, M. Tymchenko, and A. Alu, Nonlinear metasurfaces: a paradigm shift in nonlinear optics, *Mater. Today* **21**, 8 (2018).
 - [6] D. Smirnova and Y. S. Kivshar, Multipolar nonlinear nanophotonics, *Optica* **3**, 1241 (2016).
 - [7] M. Kauranen and A. V. Zayats, Nonlinear plasmonics, *Nat. Photonics* **6**, 737 (2012).
 - [8] J. Khurgin, Graphene – a rather ordinary nonlinear optical material, *Appl. Phys. Lett.* **104**, 161116 (2014).
 - [9] F. J. Garcia de Abajo and J. D. Cox, Electrically tunable nonlinear plasmonics in graphene nanoislands, *Nat. Commun.* **5**, 5725 (2014).
 - [10] G. Grinblat, Y. Li, M. P. Nielsen, R. F. Oulton,

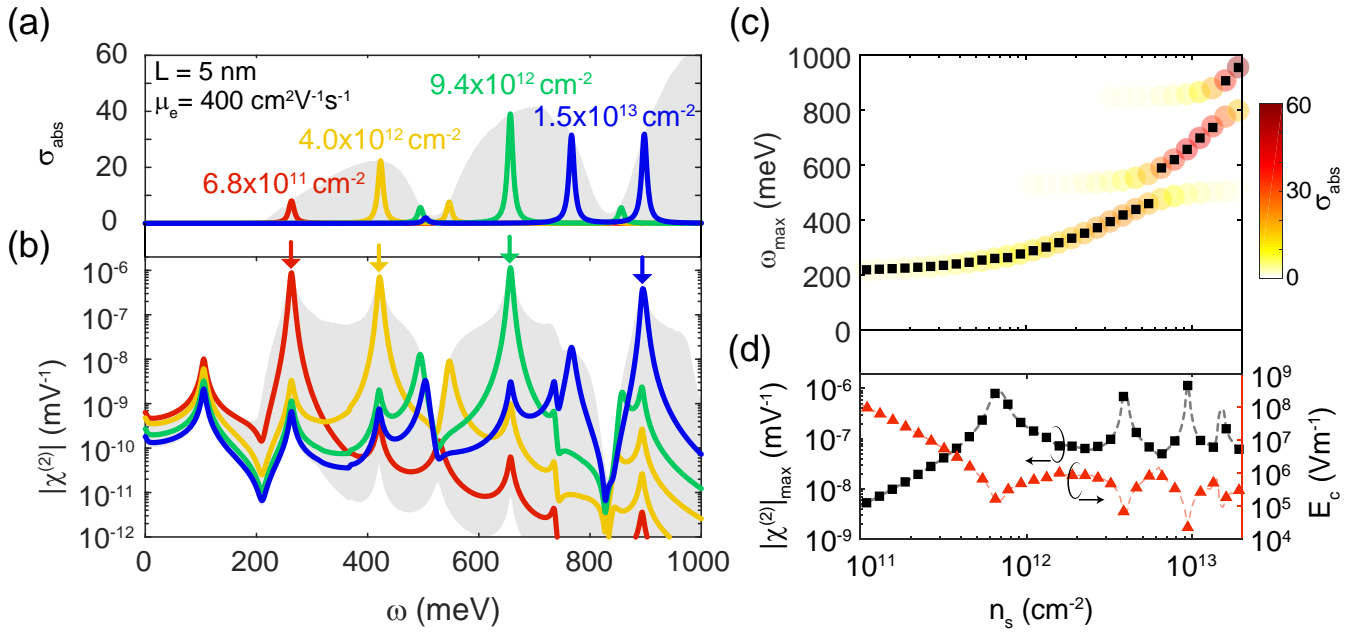


FIG. 2. (a) The loss function and (b) the second-order susceptibility ($\chi^{(2)}$) versus illumination frequency for different carrier densities. The arrow-marked peaks correspond to plasmon resonances. The gray shaded areas show σ_{abs} and $\chi^{(2)}$ calculated for carrier densities in the 10^{11} – $3 \times 10^{13} \text{ cm}^{-2}$ range. (c) ω_{max} , the frequency of maximum second-order susceptibility (square) and (d) its corresponding values of $|\chi^{(2)}|_{\text{max}}$ (square) and E_c (triangle) as a function of carrier density. The filled circles in (c) represent plasmon resonances and the color bar shows the corresponding loss function of each plasmon resonance. Note that ω_{max} coincides with a plasmon resonance. In all panels, $L = 5 \text{ nm}$ and $\mu_e = 400 \text{ cm}^2/\text{Vs}$.

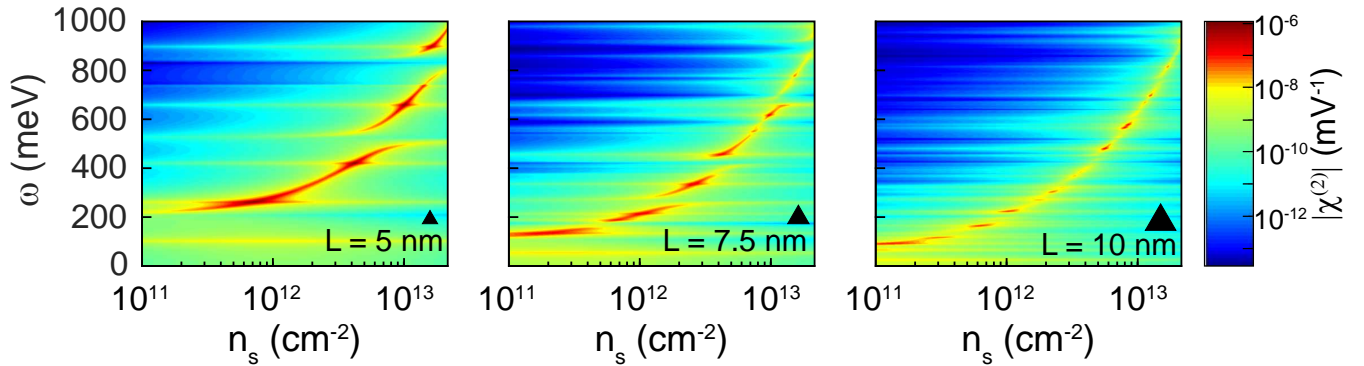


FIG. 3. The magnitude of the second-order susceptibility as a function of frequency and carrier density for an MoS₂ nanotriangle with (left) $L = 5 \text{ nm}$, (middle) $L = 7.5 \text{ nm}$, and (right) $L = 10 \text{ nm}$. Smaller nanotriangles exhibit stronger second-order nonlinear optical response.

- and S. A. Maier, Enhanced third harmonic generation in single germanium nanodisks excited at the anapole mode, *Nano Lett.* **16**, 4635 (2016), pMID: 27331867, <https://doi.org/10.1021/acs.nanolett.6b01958>.
- [11] R. Camacho-Morales, M. Rahmani, S. Kruk, L. Wang, L. Xu, D. A. Smirnova, A. S. Solntsev, A. Miroshnichenko, H. H. Tan, F. Karouta, S. Naureen, K. Vora, L. Carletti, C. De Angelis, C. Jagadish, Y. S. Kivshar, and D. N. Neshev, Nonlinear generation of vector beams from algaas nanoantennas, *Nano Letters* **16**, 7191 (2016), pMID: 27797212, <https://doi.org/10.1021/acs.nanolett.6b03525>.
- [12] D. A. B. Miller, D. S. Chemla, T. C. Damen, A. C. Gosard, W. Wiegmann, T. H. Wood, and C. A. Burrus, *Phys. Rev. B* **32**, 1043 (1985).
- [13] C. Cooperman, L. Friedman, and W. Bloss, *Appl. Phys. Lett.* **44**, 977 (1982).
- [14] S. Yuen, *Appl. Phys. Lett.* **43**, 815 (1983).
- [15] D. Ahn and S.-L. Chuang, *IEEE J. Quantum Electron.* **QE-23**, 2196 (1987).
- [16] J. Khurgin, *Phys. Rev. B* **38**, 4056 (1988).
- [17] J. Khurgin, Second-order intersubband nonlinear-optical susceptibilities of asymmetric quantum-well structures, *J. Opt. Soc. Am. B* **6**, 1673 (1989).

- [18] J. D. Cox, I. Silveiro, and F. J. García de Abajo, Quantum effects in the nonlinear response of graphene plasmons, *ACS Nano* **10**, 1995 (2016).
- [19] J. D. Cox, A. Marini, and F. J. G. De Abajo, Plasmon-assisted high-harmonic generation in graphene, *Nat. Commun.* **8** (2017).
- [20] J. D. Cox and F. J. García de Abajo, Plasmon-enhanced nonlinear wave mixing in nanostructured graphene, *ACS Photonics* **2**, 306 (2015).
- [21] F. Karimi and I. Knezevic, Plasmons in graphene nanoribbons, *Phys. Rev. B* **96**, 125417 (2017).
- [22] S. Mikhailov, Theory of the giant plasmon-enhanced second-harmonic generation in graphene and semiconductor two-dimensional electron systems, *Phys. Rev. B* **84**, 045432 (2011).
- [23] F. Karimi, A. Davoody, and I. Knezevic, Nonlinear optical response in graphene nanoribbons: The critical role of electron scattering, *Phys. Rev. B* **97**, 245403 (2018).
- [24] M. Mesch, B. Metzger, M. Hentschel, and H. Giessen, Nonlinear plasmonic sensing, *Nano Lett.* **16**, 3155 (2016).
- [25] E. Hendry, P. J. Hale, J. Moger, A. Savchenko, and S. Mikhailov, Coherent nonlinear optical response of graphene, *Phys. Rev. Lett.* **105**, 097401 (2010).
- [26] T. Gu, N. Petrone, J. F. McMillan, A. van der Zande, M. Yu, G.-Q. Lo, D.-L. Kwong, J. Hone, and C. W. Wong, Regenerative oscillation and four-wave mixing in graphene optoelectronics, *Nat. Photonics* **6**, 554 (2012).
- [27] R. Wu, Y. Zhang, S. Yan, F. Bian, W. Wang, X. Bai, X. Lu, J. Zhao, and E. Wang, Purely coherent nonlinear optical response in solution dispersions of graphene sheets, *Nano Lett.* **11**, 5159 (2011).
- [28] H. Zhang, S. Virally, Q. Bao, L. K. Ping, S. Massar, N. Godbout, and P. Kockaert, Z-scan measurement of the nonlinear refractive index of graphene, *Opt. Lett.* **37**, 1856 (2012).
- [29] N. Kumar, J. Kumar, C. Gerstenkorn, R. Wang, H.-Y. Chiu, A. L. Smirl, and H. Zhao, Third harmonic generation in graphene and few-layer graphite films, *Phys. Rev. B* **87**, 121406 (2013).
- [30] S.-Y. Hong, J. I. Dadap, N. Petrone, P.-C. Yeh, J. Hone, and R. M. Osgood Jr, Optical third-harmonic generation in graphene, *Phys. Rev. X* **3**, 021014 (2013).
- [31] N. Vermeulen, D. Castelló-Lurbe, J. Cheng, I. Pasternak, A. Krajewska, T. Ciuk, W. Strupinski, H. Thienpont, and J. Van Erps, Negative kerr nonlinearity of graphene as seen via chirped-pulse-pumped self-phase modulation, *Phys. Rev. Appl.* **6**, 044006 (2016).
- [32] S. Mikhailov, Non-linear electromagnetic response of graphene, *Europhys. Lett.* **79**, 27002 (2007).
- [33] S. A. Mikhailov, Quantum theory of the third-order nonlinear electrodynamic effects of graphene, *Phys. Rev. B* **93**, 085403 (2016).
- [34] H. Rostami and M. Polini, Theory of third-harmonic generation in graphene: A diagrammatic approach, *Phys. Rev. B* **93**, 161411 (2016).
- [35] H. Rostami, M. I. Katsnelson, and M. Polini, Theory of plasmonic effects in nonlinear optics: the case of graphene, *Phys. Rev. B* **95**, 035416 (2017).
- [36] J. Cheng, N. Vermeulen, and J. Sipe, Third order optical nonlinearity of graphene, *New J. Phys.* **16**, 053014 (2014).
- [37] J. L. Cheng, N. Vermeulen, and J. Sipe, Third-order nonlinearity of graphene: Effects of phenomenological relaxation and finite temperature, *Phys. Rev. B* **91**, 235320 (2015).
- [38] V. A. Margulis, E. Muryumin, and E. Gaiduk, Quadratic electro-optic kerr effect in doped graphene, *J. Opt.* **19**, 065505 (2017).
- [39] V. A. Margulis, E. Muryumin, and E. Gaiduk, Electric-field-induced optical second-harmonic generation in doped graphene, *Solid State Commun.* **246**, 76 (2016).
- [40] F. Karimi, A. Davoody, and I. Knezevic, Dielectric function and plasmons in graphene: A self-consistent-field calculation within a markovian master equation formalism, *Phys. Rev. B* **93**, 205421 (2016).
- [41] D. Li, W. Xiong, L. Jiang, Z. Xiao, H. Rabiee Golgir, M. Wang, X. Huang, Y. Zhou, Z. Lin, J. Song, S. Ducharme, L. Jiang, J.-F. Silvain, and Y. Lu, Multimodal nonlinear optical imaging of mos2 and mos2-based van der waals heterostructures, *ACS Nano* **10**, 3766 (2016).
- [42] R. Woodward, R. Murray, C. Phelan, R. de Oliveira, T. Runcorn, E. Kelleher, S. Li, E. de Oliveira, G. Fechine, G. Eda, and C. de Matos, Characterization of the second-and third-order nonlinear optical susceptibilities of monolayer mos2 using multiphoton microscopy, *2D Mater.* **4**, 011006 (2016).
- [43] R. Wang, H.-C. Chien, J. Kumar, N. Kumar, H.-Y. Chiu, and H. Zhao, Third-harmonic generation in ultrathin films of mos2, *ACS Appl. Mater. Interfaces* **6**, 314 (2013).
- [44] A. Säynätjoki, L. Karvonen, H. Rostami, A. Autere, S. Mehravar, A. Lombardo, R. A. Norwood, T. Hasan, N. Peyghambarian, H. Lipsanen, K. Kieu, A. C. Ferrari, M. Polini, and Z. Sun, Ultra-strong nonlinear optical processes and trigonal warping in mos₂ layers, *Nat. Commun.* **8** (2016).
- [45] A. Saynatjoki, L. Karvonen, J. Riikonen, W. Kim, S. Mehravar, R. A. Norwood, N. Peyghambarian, H. Lipsanen, and K. Kieu, Rapid large-area multiphoton microscopy for characterization of graphene, *ACS Nano* **7**, 8441 (2013).
- [46] Y. Li, Y. Rao, K. F. Mak, Y. You, S. Wang, C. R. Dean, and T. F. Heinz, Probing symmetry properties of few-layer mos2 and h-bn by optical second-harmonic generation, *Nano Lett.* **13**, 3329 (2013).
- [47] A. Autere, H. Jussila, Y. Dai, Y. Wang, H. Lipsanen, and Z. Sun, Nonlinear optics with 2d layered materials, *Adv. Mater.* **30**, 1705963 (2018).
- [48] X. Wen, Z. Gong, and D. Li, Nonlinear optics of two-dimensional transition metal dichalcogenides, *InfoMat* **1**, 317 (2019), <https://onlinelibrary.wiley.com/doi/pdf/10.1002/inf2.12024>.
- [49] G. Wang, A. Chernikov, M. M. Glazov, T. F. Heinz, X. Marie, T. Amand, and B. Urbaszek, Colloquium: Excitons in atomically thin transition metal dichalcogenides, *Rev. Mod. Phys.* **90**, 021001 (2018).
- [50] G. Wang, X. Marie, I. Gerber, T. Amand, D. Lagarde, L. Bouet, M. Vidal, A. Balocchi, and B. Urbaszek, Giant enhancement of the optical second-harmonic emission of wse₂ monolayers by laser excitation at exciton resonances, *Phys. Rev. Lett.* **114**, 097403 (2015).
- [51] K. J. Lee, W. Xin, C. Fann, X. Ma, F. Xing, J. Liu, J. Zhang, M. Elkabbash, and C. Guo, Exciton dynamics in two-dimensional Mos₂ on a hyperbolic metamaterial-based nanophotonic platform, *Phys. Rev. B* **101**, 041405 (2020).
- [52] A. Taghizadeh and T. G. Pedersen, Nonlinear optical selection rules of excitons in monolayer transition metal

- dichalcogenides, *Phys. Rev. B* **99**, 235433 (2019).
- [53] S. Xie, L. Tu, Y. Han, L. Huang, K. Kang, K. U. Lao, P. Poddar, C. Park, D. A. Muller, R. A. DiStasio, *et al.*, Coherent, atomically thin transition-metal dichalcogenide superlattices with engineered strain, *Science* **359**, 1131 (2018).
- [54] H. Wang, D. Zhu, F. Jiang, P. Zhao, H. Wang, Z. Zhang, X. Chen, and C. Jin, Revealing the microscopic cvd growth mechanism of mose2 and the role of hydrogen gas during the growth procedure, *Nanotechnology* **29**, 314001 (2018).
- [55] J. Lauritsen, M. Bollinger, E. Lægsgaard, K. W. Jacobsen, J. K. Nørskov, B. Clausen, H. Topsøe, and F. Besenbacher, Atomic-scale insight into structure and morphology changes of mos2 nanoclusters in hydrotreating catalysts, *J. Catal.* **221**, 510 (2004).
- [56] A. Tuxen, J. Kibsgaard, H. Gøbel, E. Lægsgaard, H. Topsøe, J. V. Lauritsen, and F. Besenbacher, Size threshold in the dibenzothiophene adsorption on mos2 nanoclusters, *ACS Nano* **4**, 4677 (2010).
- [57] S. Helveg, J. V. Lauritsen, E. Lægsgaard, I. Stensgaard, J. K. Nørskov, B. Clausen, H. Topsøe, and F. Besenbacher, Atomic-scale structure of single-layer mos 2 nanoclusters, *Phys. Rev. Lett.* **84**, 951 (2000).
- [58] R. Schiek and T. Pertsch, Absolute measurement of the quadratic nonlinear susceptibility of lithium niobate in waveguides, *Opt. Mater. Express* **2**, 126 (2012).
- [59] F. A. Rasmussen and K. S. Thygesen, Computational 2d materials database: electronic structure of transition-metal dichalcogenides and oxides, *J. Phys. Chem. C* **119**, 13169 (2015).
- [60] S. Khorasani, Third-order optical nonlinearity in two-dimensional transition metal dichalcogenides, *Communications in Theoretical Physics* **70**, 344 (2018).
- [61] H. Rostami, R. Roldán, E. Cappelluti, R. Asgari, and F. Guinea, Theory of strain in single-layer transition metal dichalcogenides, *Phys. Rev. B* **92**, 195402 (2015).
- [62] E. Cappelluti, R. Roldán, J. A. Silva-Guillén, P. Ordejón, and F. Guinea, Tight-binding model and direct-gap/indirect-gap transition in single-layer and multilayer mos₂, *Phys. Rev. B* **88**, 075409 (2013).
- [63] W. Gaddah, A Lie group approach to the Schrödinger equation for a particle in an equilateral triangular infinite well, *European Journal of Physics* **34**, 1175 (2013).
- [64] W. Li and S. M. Blinder, Solution of the Schrödinger equation for a particle in an equilateral triangle, *Journal of Mathematical Physics* **26**, 2784 (1985), <https://doi.org/10.1063/1.526701>.
- [65] B. Radisavljevic, A. Radenovic, J. Brivio, i. V. Giacometti, and A. Kis, Single-layer mos 2 transistors, *Nat. Nanotechnol.* **6**, 147 (2011).
- [66] K. Kaasbjerg, K. S. Thygesen, and K. W. Jacobsen, Phonon-limited mobility in n-type single-layer mos 2 from first principles, *Phys. Rev. B* **85**, 115317 (2012).
- [67] Q. H. Wang, K. Kalantar-Zadeh, A. Kis, J. N. Coleman, and M. S. Strano, Electronics and optoelectronics of two-dimensional transition metal dichalcogenides, *Nat. Nanotechnol.* **7**, 699 (2012).
- [68] M. Lundstrom, *Fundamentals of Carrier Transport*, 2nd ed. (Cambridge University Press, Cambridge, 2000).